中國機械工程學刊第四十六卷第一期第 41~49 頁(民國一百一十四年)
Journal of the Chinese Society of Mechanical Engineers, Vol.46, No.1, pp41~49 (2025)

Developing an Automatic Measuring Instrument for the Prismatic Refractive Power of Lenses

Ching-Huang Lin*, Cheng-Chung Lee**, Wen-Hong Wu***, Fu-Kuei Chan****and Shun-Yuan Chien*****

Keywords: eyewear testing, image processing, prismatic refractive power

ABSTRACT

With improvements in quality of life, the demand for high-quality safety glasses and sunglasses has increased. Prismatic refractive power is a crucial aspect of eyewear testing. According to ISO 18526-1:2020, this testing procedure involves focusing an inspection beam on a scale target 2 m away after it passes through the glasses. Subsequently, the prismatic refractive power of the lenses is determined by observing the displacement of the focal point. Nevertheless, human observation errors may occur during testing. Therefore, in this study, a machine vision module was developed to obtain target images, and image processing and recognition techniques were used to automatically determine the position of the focused spot of light and calculate each lens's prismatic refractive power. This instrument eliminates the need for human observation, manual calculation, and record-keeping, and it reduces the workforce required for inspection.

Paper Received September, 2023. Revised May, 2024. Accepted July, 2024. Author for Correspondence: Cheng-Chung Lee

** Department of Electronic Engineering, National Yunlin University of Science and Technology, Yunlin, Taiwan, 640, ROC*

*** Graduate School of Engineering Science and Technology, National Yunlin University of Science and Technology, Yunlin, Taiwan, 640, ROC, @gmail.com*

**** Taiwan Instrument Research Institute, National Applied Research Laboratories, Hsinchu, Taiwan, 300, ROC*

***** YIN-TSUNG Co., Ltd., Tainan, Taiwan, 717, ROC*

****** Hardline Laboratory, SGS Taiwan Ltd., Kaohsiung, Taiwan, 806, ROC.*

INTRODUCTION

In recent years, the role of eyewear has evolved from a functional necessity to a personal accessory, leading to a substantial increase in the demand for various types of eyewear. The requirements for the quality of safety glasses and sunglasses have been enhanced, particularly in light of the COVID-19 pandemic. Various types of glasses are available, including prescription glasses, safety glasses, and sunglasses. Prismatic refractive power is an essential aspect of sunglasses and safety glasses because it influences the wearer's clarity of vision. In eyewear, prism effects can cause visual fatigue and reading discomfort, making prismatic refractive power a key component in lens quality testing. Prismatic refractive power results from the eccentricity or tilt of the optical axis of the lens. Currently, eyewear testing is primarily conducted in accordance with Clause 6.2 of ISO 18526-1:2020. This standard involves passing light through the center of the lens and focusing this light on a scale target located 2 m away (Fig. 1). If the lens exhibits no prism deviation, the three light beams passing through aperture A converge at a single point. By contrast, if the lens exhibits prism deviation, these beams do not focus on the same point. To calculate the prismatic deviation of a lens, the positions of and distances between the light spots on the scale target are measured. Traditionally, to avoid frequent movement between the lens and the target, a two-person approach is employed. One person positions the lens, whereas the other person observes and records the positions and distances of the light spots on the scale target. Despite the benefits of this approach, manual observation may introduce errors due to operator fatigue or emotion fluctuation. Therefore, to overcome these challenges, machine vision was used in this study instead of human visual observation. In addition, image processing and recognition techniques were used to automatically identify the positions of focused light spots and calculate a lens's prismatic refractive power. This technique enables the automation of prismatic refractive power testing for eyewear lenses, thereby substantially reducing operator errors and increasing testing efficiency.

Dimensions in millimetres (nominal unless toleranced)

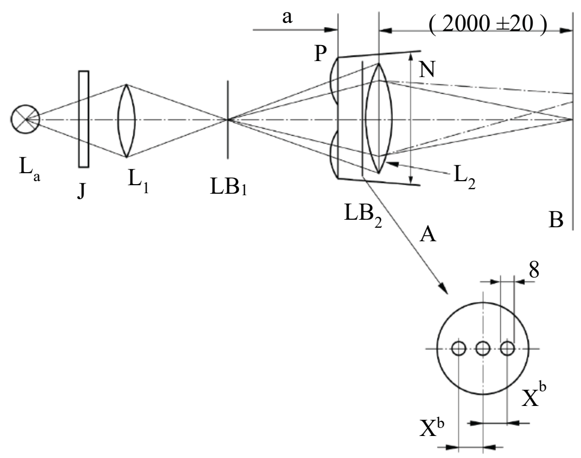

L_a	light source (e.g., a small filament lamp or a laser with a wavelength of 600 ± 70 nm)
L_1	lens with a focal length of 20–50 mm
LB_1	diaphragm with a nominal aperture diameter of 1 mm
P	test sample
LB_2	diaphragm as indicated by label A
L_2	lens with a nominal focal length of 1000 mm and a nominal diameter of 75 mm
B	image plane
a	distance between the test sample and lens L2, which should be minimal
X^b	half of the distance between pupils, as defined by the headforms specified in ISO 18526-4
N	superior attachment of the pinna breadth, as defined by the headforms specified in ISO 18526-4
J	filter with peak transmittance in the green section of the spectrum (required only if a filament lamp is used as the light source)

Fig. 1 Prismatic Refractive Power Measurement Framework in ISO 18526-1:2020

MEASUREMENT OF PRISMATIC REFRACTIVE POWER FOR EYEWEAR LENSES

In an eyeglass lens, prismatic difference refers to the deflection of incident light as it exits the lens due to the displacement or tilt of the lens. As shown in Fig. 2, when a collimated beam of light passes along the axis of a convex lens, the focal point converges onto the lens's axis (Fig. 2A). If the lens is shifted downward or the collimated beam of light enters from above the lens center (Fig. 2B), the focal point appears below the center axis of the light beam. By contrast, if the lens is shifted upward or the collimated beam of light enters from below the lens center, the focal point is positioned above the center axis of the incident beam (Fig. 2C). Lens displacement and tilt influence the position of the focal point, yielding similar effects. If the lenses of sunglasses or safety glasses are displaced or tilted, a deviation occurs in the line of sight, which may influence visual judgment. This deviation is referred to as prismatic deviation, and it is measured in terms of prismatic refractive power.

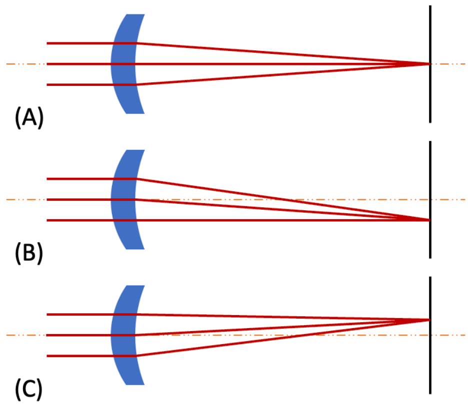

Fig. 2 Cases of Prismatic Deviation

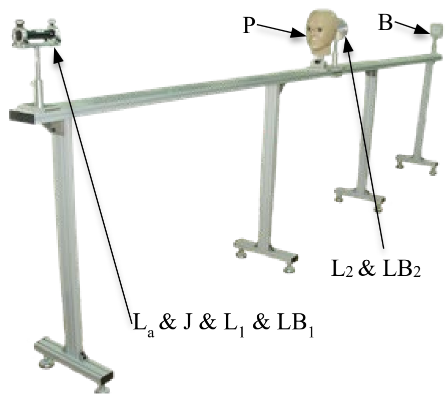

Fig. 3 Instrument Used for Measuring Prismatic Refractive Rower

According to ISO 4007:3.7.12, prismatic refractive power is defined as the deviation of light by 1 cm at a distance of 1 m, and it is measured in units of centimeters per meter. The following is the formula employed to calculate the prismatic refractive power:

$$\text{Prismatic refractive power} = \frac{\text{Deviation (in cm)}}{\text{Distance (in m)}} \qquad (1)$$

Fig. 3 depicts the setup used for measuring the prismatic refractive power of multiple lenses. After the lenses to be tested were placed on a head form (Fig. 3, middle), a laser beam was passed through these lenses, focused by a converging lens labeled L2 (Fig. 1), and projected onto a scale target (Fig. 3, right). Fig. 4 presents an example of the prismatic refractive power of a scale target image. Each small grid square on the scale target was of size 0.1 cm. To calculate prismatic refractive power, the deviation of the focused light spot was determined. As shown in Fig. 4, the left laser focus spot deviated by a single grid on the target, indicating a deviation of 0.1 cm. Because the scale target was placed at a distance of 2 m, the prismatic refractive power was thus 0.05 cm/m.

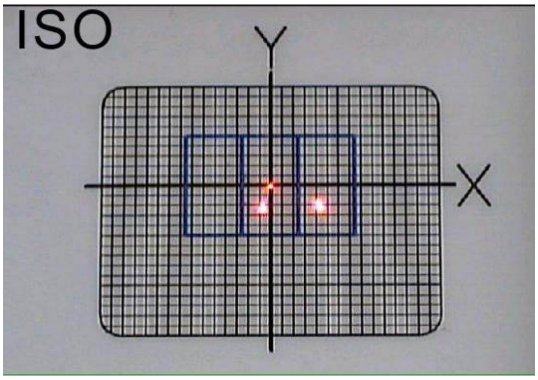

Fig. 4 Prismatic Refractive Power of a Scale Target

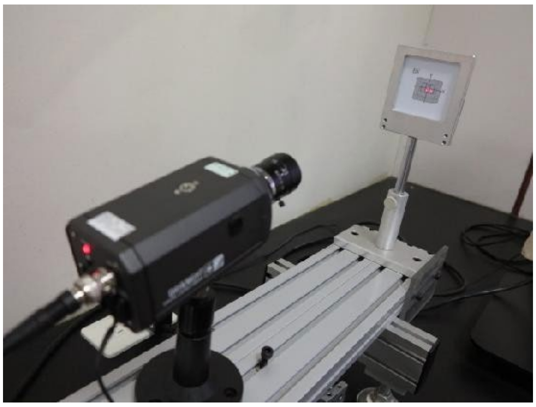

Fig. 5 Image Acquisition Module

AUTOMATED INSTRUMENT FOR PRISMATIC REFRACTIVE POWER MEASUREMENT

This section details the development of an automatic instrument for measuring the prismatic refraction power of lenses. In addition to a machine vision module, image prepositioning, image processing and recognition, and prismatic refraction power calculation are used.

Image Acquisition Module

In this study, the horizontal length of the calibration grid was set to 20 mm on the scale target, and the imaging range was then set to 30 mm. In addition, the minimum width of the finest grid line was set to approximately 0.1 mm, and the minimum number of pixels required to resolve the finest grid line was calculated as 600. To accelerate processing, a camera with resolution of 640 × 480 pixels was used to obtain smaller images. A general closed-circuit television (CCTV) lens was used to obtain images. Fig. 5 depicts the image acquisition module.

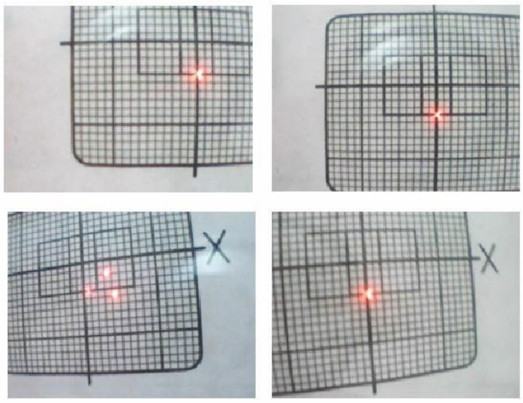

Fig. 6 Image Acquisition without Prealignment

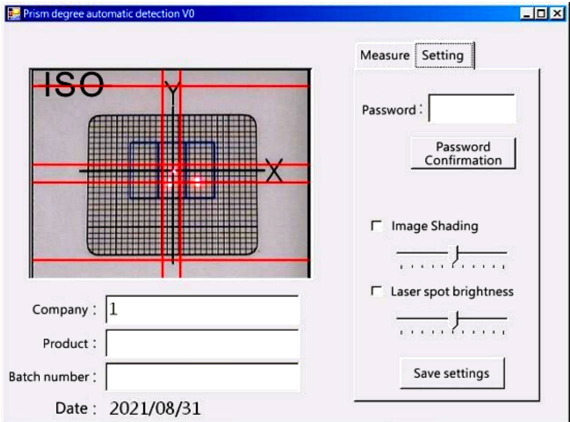

Fig. 7 Human–Machine Interface for Image Prepositioning

Image Positioning

If the image of the scale target is outside the acquisition frame (Fig. 6, top), the laser focus spot may not appear within the acquisition image. Therefore, the center of the scale target must be aligned with the center of the acquisition image.

If the optical axis of the image lens (CCTV lens) is not perpendicular to the scale target, the image of the scale target appears tilted and distorted (Fig. 6, bottom), and the grid size varies. Generally, distorted images should be calibrated using image processing techniques. In this study, to minimize the development time of image processing software, image prepositioning was performed. On the user interface of the automatic measurement instrument, the user is guided to adjust the position of the imaging module (Fig. 7). A red reference line is subsequently drawn in the image display area of the setting page. The user adjusts the position of the imaging module to ensure that the crosshair of the calibration target center is located in the area outlined by the red reference line and to guarantee that the bottom edge of the calibration target image is close to the lower red reference line and is horizontal. This technique enables the acquisition of images with consistent quality for subsequent processing.

Image Processing: Grid Line Localization

Grid positioning on a scale target can be achieved using edge detection techniques in image processing. In addition to first-order differentiation of image gray values, techniques such as Laplacian, Marr–Hildreth, and Canny operators can be employed to identify edges. Fig. 5 shows the image obtained by the imaging module, which contains red, green, and blue areas. Fig. 4 depicts the original image, which was later processed to obtain a gray image (Fig. 8A).

The following is the formula used to calculate contrast enhancement:

$$\Psi_{i,j} = \begin{cases} 255, \ \text{for } \Phi_{i,j} > I_H \\ \frac{\Phi_{i,j} - I_L}{I_H - I_L} \times 255, \ \text{for } I_L \le \Phi_{i,j} \le I_H \\ 0, \ \text{for } \Phi_{i,j} < I_L \end{cases} \qquad (2)$$

where $\varphi_{i,j}$ and $\psi_{i,j}$ are the grayscale values of pixels at coordinates (i, j) in the original image and contrast-enhanced image, respectively, and I_H and I_L are the upper and lower thresholds of contrast enhancement, respectively, which were set to 60 and 190, respectively, in this study. Fig. 8B shows the contrast-enhanced image.

For the scale target, edge and centerline detection is performed by identifying rapid changes in the grayscale values of image pixels along the horizontal lines $Y = 160$ and $Y = 360$ and vertical lines $X = 160$ and $X = 480$. The detected edge points are indicated by blue circles in Fig. 8C. The edges of the scale target lines are determined. Given that the size of the image is predetermined during the initial localization process, the width of the scale target line image is already known. Therefore, the center point of each scale target line is marked using an offset, as indicated by the green cross in Fig. 8C.

Utilizing the same technique to search along the horizontal lines $Y = 90$ and $Y = 440$ and vertical lines $X = 90$ and $X = 480$ leads to identification of the locations of the Y-axis and X-axis, respectively. Once the position of the center point of the scale target line has been determined, the relationship between the scale of the scale target and the image pixels can be established to facilitate subsequent calculations of prismatic refractive power. The intersection of the horizontal and vertical center lines of the scale target is defined as a reference for prismatic refractive power calculations.

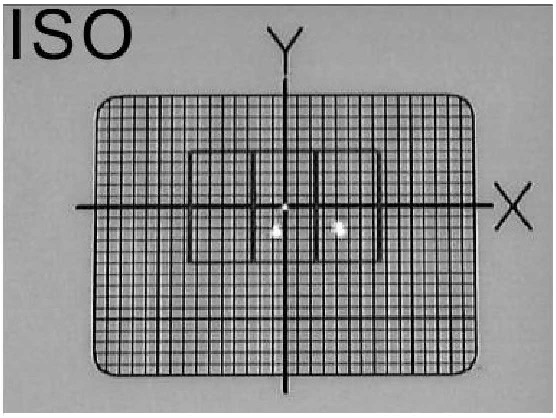

(A)

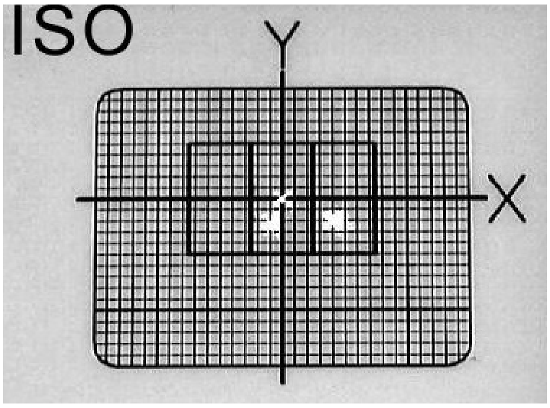

(B)

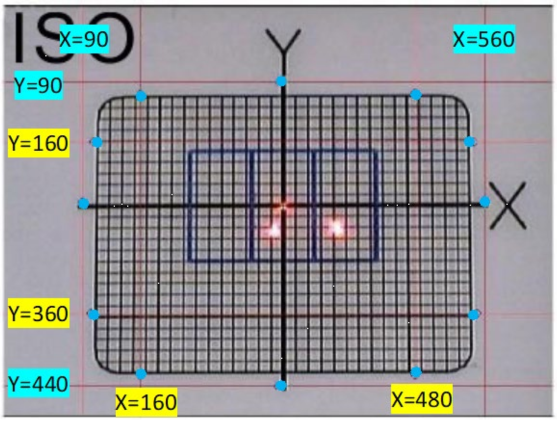

(C)

Fig. 8 Image with Grid Positioning

Image Processing: Focused Spot Localization

Fig. 5 shows the image captured by the imaging module. Although a red laser was used for measurement, the laser light was scattered at the edge of the laser spot. Nevertheless, the red light image clearly depicted the phenomenon of scattered laser spot edges, which was not conducive to determining the center of the focused spot. Cameras typically have a filter in front of their photosensitive element (e.g., charge-coupled device or complementary metal oxide semiconductor) to generate three channels (red, green, and blue) and obtain a color image. In principle, the red laser light does not appear in the green image. However, laser spots are highly focused and have high brightness. Therefore, these spots produce overexposure not only in the red image but also in the green and blue images. Because blue light has a short wavelength, the blue image is affected by stray light. Therefore, in focused spot localization, the green image is used (Fig. 8A). The following are the steps of focused spot localization.

Image Binarization: In this step, the overexposed and nearly overexposed parts of an image are highlighted to extract a laser spot image from the entire image. In the following binarization formula, $\Phi_{i,j}$ represents the original image, $\Psi_{i,j}$ represents the enhanced image, and q is the binarization threshold value, which was set to 240 in this study.

$$\Psi_{i,j} = \begin{cases} 255, & \text{for } \Phi_{i,j} \geq 240 \\ 0, & \text{for } \Phi_{i,j} < 240 \end{cases} \quad (3)$$

Search of a laser focused spot image area: In this step, the composition of pixels in the image is used to determine the range and number of graphic blocks depending on their connectivity. In this example, an area with a grayscale value of 255 was searched in a binary image, and each area was separated depending on its connectivity (Fig. 9A).

Calculation of laser focused spot center (P_x, P_y): In this step, the centroid position of each connected area is calculated using the following formula and marked as the center point of the laser focused spot (Fig. 9A):

$$P_x = \frac{\sum_{each\ pixel\ in\ the\ connected\ area} x_i}{number\ of\ pixels\ in\ the\ connected\ area}$$

$$P_y = \frac{\sum_{each\ pixel\ in\ the\ connected\ area} y_i}{number\ of\ pixels\ in\ the\ connected\ area} \quad (4)$$

where x_i and y_i represent the pixel coordinates of each pixel in the connected area. Fig. 9(B) presents a zoomed-in image of the focused spot, in which the red dot indicates the center point of each focused spot area. This red dot is located at the corresponding position on the target image (Fig. 9C).

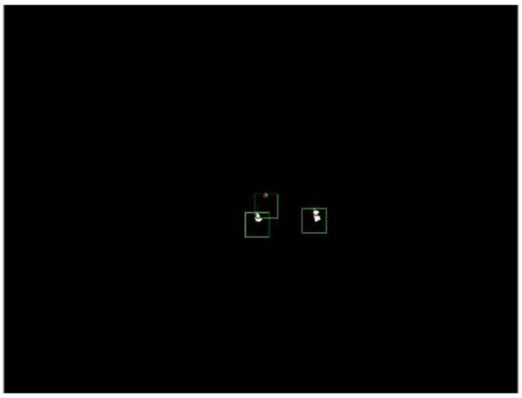
(A)

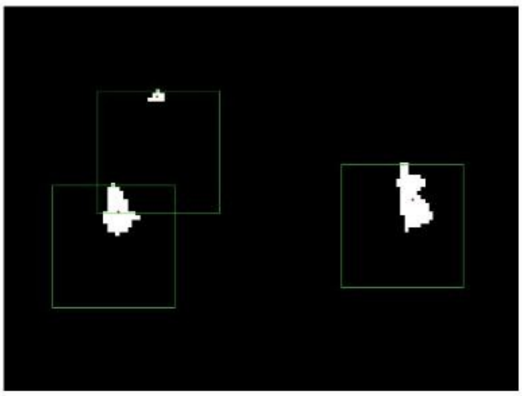
(B)

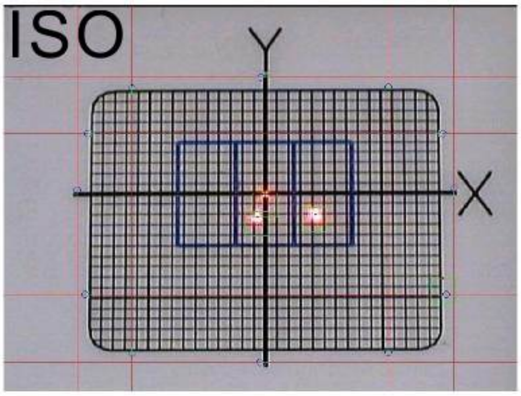

(C)

Fig. 9 Focused Spot Area on an Image

Calculation of Prismatic Refractive Power

In this calculation process, the first step is to determine the rate of conversion between pixels in the images of the scale target and the actual distance in the scale target.

Fig. 10 depicts the pixel coordinates of the center of the scale target boundary and the center point of the scale target. As indicated by the pixel coordinates, the target image was slightly tilted and deformed, with an error of approximately 1 pixel caused by tilt. To avoid intersection with the laser beam, the imaging module was installed at a low position, and the target image was captured from bottom to top. Therefore, in the horizontal direction, the lower part of the target image was approximately 8 pixels wider than the upper part. Target images should generally be corrected using an image distortion correction technique to increase measurement accuracy. In this study, to minimize the image processing software development time, an interpolation correction method was conducted during the conversion between pixel measurements and actual distances. The following formula can be used to calculate the conversion rates, $r_{x,160}$ and $r_{x,360}$, between horizontal pixels and actual length at Y-coordinates of 160 and 360, respectively:

$$r_{x,160} = \frac{X_{160,2} - X_{160,1}}{L_x}$$

$$r_{x,360} = \frac{X_{360,2} - X_{360,1}}{L_x} \qquad (5)$$

where $r_{x,160}$ represents the pixel to actual length (in mm) conversion rate on the horizontal line $Y = 160$ in pixel coordinates; $X_{160,1}$ and $X_{160,2}$ represent the X pixel coordinate values of the left and right intersection points, respectively, between the horizontal line $Y = 160$ and the edges of the target grid lines; L_x represents the actual height of the scale target (30 mm in this case); $r_{x,360}$ represents the pixel to actual length (in mm) conversion rate on the horizontal line $Y = 360$ in pixel coordinates; and $X_{360,1}$ and $X_{360,2}$ represent the X pixel coordinate values of the left and right intersection points, respectively, between the horizontal line $Y = 360$ and the edges of the target grid lines.

In Fig. 10, $X_{160,2}$ = 543, $X_{160,1}$ = 110, $X_{360,2}$ = 547, and $X_{360,1}$ = 107, with $r_{x,160}$ = 14.4, $r_{x,360}$ = 14.67, and r_x = 14.55 calculated using formula (5).

The following formula can be used to calculate the average conversion rate r_y between the vertical pixels in the image and the actual length (in mm):

$$r_y = \frac{(Y_{160,2} - Y_{160,1}) + (Y_{480,2} - Y_{480,1})}{L_y * 2} \qquad (6)$$

where $Y_{160,1}$, $Y_{160,2}$, $Y_{480,1}$, and $Y_{480,2}$ represent the Y pixel coordinate values of the left and right intersection points between the vertical lines $X = 160$ and $X = 480$ and the edges of the target grid lines and L_y is the actual height of the scale target (25 mm in this case).

In Fig. 10, $Y_{160,2}$ = 430, $Y_{160,1}$ = 107, $Y_{480,2}$ = 429, and $Y_{480,1}$ = 105, with r_y = 12.94 calculated using formula (6).

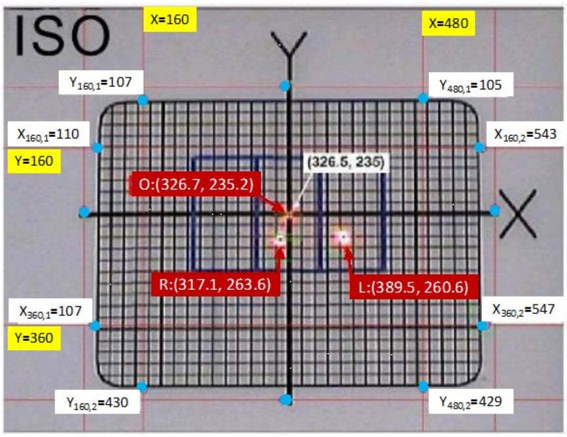

Fig. 10 Target Image and Measurement Data for Test Eyeglasses

Prism measurements are typically conducted through visual observation; thus, the precision of the laser focusing point did not need to be high. In addition, the tilted screen resulted in a negligibly small error, and only image deformation error correction was required. Fig. 10 shows the pixel coordinates of the laser focus point center. The pixel coordinates of the center focus point O were (O_x, O_y) = (326.7, 235.2), and the pixel coordinates of the right lens focus point R were (R_x, R_y) = (317.1, 263.6). Therefore, the horizontal pixel offset $\triangle_x$ and vertical pixel offset $\triangle_y$ of the right lens of the test eyeglasses were 9.6 and 28.4 pixels, respectively. The following interpolation formula was used to calculate the actual length conversion rate r_x for horizontal pixels:

$$r_x = r_{x,160} + \frac{0.5\times(O_y+R_y)-160}{360-160} \times \left(r_{x,360} - r_{x,160}\right) \tag{7}$$

After r_x was calculated as 14.62, the following formulas were used to calculate the actual horizontal offset δ_x, vertical offset δ_y, and total offset of the focus point:

$$\delta_x = \frac{\Delta_x}{r_x}$$
$$\delta_y = \frac{\Delta_y}{r_y} \tag{8}$$
$$\delta = \sqrt{\delta_x^2 + \delta_y^2}$$

According to the results, the horizontal and vertical prism deviations of the right lens of the test glasses were $\delta_x = 0.66$ and $\delta_y = 2.19$, respectively, with a total deviation δ of 2.29 mm. These measured deviations of the focus point were consistent with the visual findings. After the prismatic refractive power of the right lens of the test glasses was calculated as 0.1145 cm/m, the pixel coordinates of the left lens focus point L were determined as (L_x, L_y) = (389.5, 260.6), with horizontal and vertical pixel deviations of 62.8 and 25.4 pixels, respectively. After the value of r_x was calculated as 14.54, the horizontal and vertical prism deviations were determined as $\delta_x = 4.32$ and $\delta_y = 1.96$, respectively, with a total deviation δ of 4.74 mm and a prismatic refractive power of 0.237 cm/m.

Fig. 11 depicts the test results obtained for the second pair of glasses, including the captured target image and measurement data. The right lens of the second pair of glasses exhibited a horizontal shift of 61.7 pixels and a vertical shift of 5.1 pixels. After the values of $r_{x,160}$ and $r_{x,360}$ were calculated as 14.47 and 14.70, respectively, the values of r_y and r_x were calculated as 12.96 and 14.56, respectively. These results indicated that the horizontal and vertical prism deviations of the right lens of the second pair of glasses were $\delta_x = 4.24$ and $\delta_y = 0.39$, respectively, with a total deviation δ of 5.26 mm. After the horizontal and vertical shifts of the left lens of the second pair of glasses were calculated as 98.6 and 10.1 pixels, respectively, the values of r_y and r_x were determined as 12.96 and 14.55, respectively. These results indicated that the horizontal and vertical prism deviations of the left lens of the second pair of glasses were $\delta_x = 6.78$ and $\delta_y = 0.78$, respectively, with a total deviation δ of 6.82 mm. Overall, the measured values of prism deviation for the two lenses of the second pair of glasses were consistent with the visual findings. The prismatic refractive power of the right and left lenses of the second pair of glasses was calculated using formula (1) as 0.213 and 0.341 cm/m, respectively.

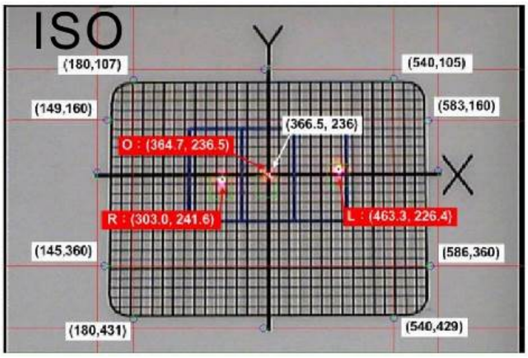

Fig. 11 Target Image and Measurement Data for the Second Pair of Glasses

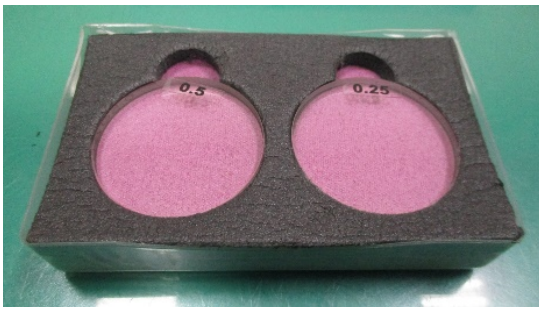

Fig. 12 Two Calibrated Prism Lenses

Instrument Calibration

The power of the prisms was calibrated through a comparison method involving the use of two power lenses already calibrated by the British National Physical Laboratory; the calibration process involved 33 measurements (Fig. 12). Table 1 presents the measurement results. In accordance with Clause 6.2.2 of ISO 18526-1, measurements with a standard deviation(SD) of 0.05 or less are regarded as acceptable. As indicated by Table 1, the measurements of the proposed instrument were acceptable.

Table 1 Measurement Results

	0.25Δ	0.5Δ
Prisms	0.266Δ	0.494Δ
Tolerance	≦0.05	≦0.05

Max.	0.266	0.494
Min.	0.261	0.489
Average	0.264	0.491
SD.	0.0015	0.0019

CONCLUSION AND SUGGESTIONS

In recent years, the preference for eyewear among people in Taiwan has evolved from functional use to a personal accessory. This shift has resulted in a substantial increase in the demand for various types of eyewear, accompanied by increased quality expectations. Despite these changes, most optical inspection instruments still rely on manual observation, which typically requires the involvement of two or more individuals. This approach is not only time-consuming but also prone to quality variability. In this study, an automated instrument was developed that can measure the prismatic refractive power of lenses. This instrument utilizes machine vision technology instead of manual observation to mitigate errors caused by eye fatigue and reduce occupational hazards linked to prolonged exposure to high-intensity light spots. Image processing technology is used to analyze images and automate the measurement of prismatic refractive power, thereby mitigating potential errors in manual observation, recording, and calculation; eliminating the need for human inspection; and substantially increasing the efficiency of inspection. Two lenses were used to evaluate the effectiveness of the proposed instrument. The results were found to be consistent with those of manual inspection and were even more accurate. Overall, the proposed instrument can be used as a feasible alternative to manual inspection and can greatly contribute to the advancement of the eyewear inspection industry. It can also serve as a future reference for ISO 18526-1 with machine vision for inspection.

ACKNOWLEDGMENTS

The authors would like to thank the Taiwan Instrument Research Institute, National Applied Research Laboratories, for the technical support.

REFERNCES

Abdelali Taatali, Sif Eddine Sadaoui, Mohamed Abderaouf Louar & Brahim Mahiddini, "On-machine dimensional inspection: machine vision-based approach", Springer Link(2024).

Aznar-Casanova JA, Romeo A, Gómez AT, Enrile PM," Visual fatigue while watching 3D stimuli from different positions", J Optom,10(3):149-160. doi: 10.1016/j.optom.2016.07.002. Epub 2016 Aug 17. PMID: 27544414; PMCID: PMC5510554 (2017 Jul-Sep.).

Davies E.R., "Machine Vision Theory Algorithms Practicalities", pp 161-165, Elsevier Inc (2005).

Devyani Bhamare, Poonam Suryawanshi, "Review on Reliable Pattern Recognition with Machine Learning Techniques", Taylor & Francis (2019).

Gnozalez R.C., Woods R. E., "Digital Image Processing", pp 572-586, Prentice-Hall Inc (2002).

Grzegorz Owczarek, Adam Pościk, Zygmunt Kubacki & Maciej Karolewski,"The Relationship Between the Difference in Prismatic Refractive Power of an Eye-and-Face Protector and Its Thickness", Radius of Curvature, and Material, International Journal of Occupational Safety and Ergonomics, 7:3, 277-284, DOI: 10.1080/10803548.2001.11076491 (2001).

Health and Environment Sector Policy and Strategy Committee, "EN 167-2002 Personal eye-protection-Optical test methods", British Standard, ISBN 0-580-38915-4 (2002).

Husein Perez andJoseph H. M. Tah, "Towards Automated Measurement of As-Built Components Using Computer Vision", MDPI(2023).

International Safety Equipment Association, "ANSI / ISEA Z87.1-2020 American National Standard for Occupational and Educational Personal Eye and Face Protection Devices", American National Standards Institute, Inc., 9.5.1~9.5.3 p.20 (2020).

ISO/TC 94, "ISO 4007 Personal protective equipment - Eye and Face Protection - Vocabulary", ISO copyright office (2018).

ISO/TC 94, "ISO 18526-1:2020 Eye and face protection - Test methods - Part 1: Geometrical optical properties", ISO copyright office (2020).

ISO/TC 94, "ISO 18526-4:2020 Eye and face protection - Test methods - Part 4: Headforms", ISO copyright office (2020).

Iqbal H. Sarker, Machine Learning: Algorithms,

"Real-World Applications and Research Directions", Springer Link (2021).
KC Santosh, "Current Trends in Image Processing and Pattern Recognition", Fronties, Editorial (2021).
LIN, QING-HUANG and KE, MING-DA, and LI, ZHENG-ZHONG, "Prism diopter tester", Patent Number:109129353, March.1. (2022).
Masoud Shaloo, Gábor Princz & Selim Erol, "Real-Time Color Detection for Automated Production Lines Using CNN-Based Machine Learning", Springer Link (2024).
M. Partio, B. Cramariuc and M. Gabbouj, "An Ordinal Cooccurrence Matrix Framework for Texture Retrieval", EURASIP Journal on Image and Video Processing, Volume 2007, Article ID 17358 (2007).
NATIONAL PHYSICAL LABORATORY, "ertificate of calibration-six test lenses & two prisms", (2022).
Pin Wang, En Fan, Peng Wang, "Comparative analysis of image classification algorithms based on traditional machine learning and deep learning", Elsevier Inc, Pattern Recognition Letters Volume 141, Pages 61-67(2021).
Posada J, Toro C, Barandiaran I, Oyarzun D, Stricker D, De Amicis R, Pinto EB, Eisert P, Dollner J, Vallarino I, "Visual computing as a key enabling technology for Industrie 4.0 and industrial internet". IEEE Comput Grap Appl 35:26–40 (2015).
R. M. Haralick, K. Shanmugam and I. Dinstein, "Tectural Features for Image Classification", IEEE Transactions on Systems, Man, and Cybernetics, Vol. SMC-3 No.6, pp. 610-621 (1973).
Rong-Qing Qiu, Mu-Lin Tsai, Yu-Wen Chen, Shivendra Pratap Singh and Cheng-Yao Lo, "Integrated Automatic Optical Inspection and Image Processing Procedure for Smart Sensing in Production Lines", MDPI (2024).
Stavis M, Murray M, Jenkins P, Wood R, Brenham B, Jass J. "Objective improvement from base-in prisms for reading discomfort associated with mini-convergence insufficiency type exophoria in school children". Binocul Vis Strabismus Q. ,17(2):135-42. PMID: 12067271 (2002).
Wei-Chien Wang; Shang-Liang Chen; Liang-Bi Chen; Wan-Jung Chang, "A Machine Vision Based Automatic Optical Inspection System for Measuring Drilling Quality of Printed Circuit Boards", IEEE (2016).
Yunqing Bai,Jihong Pei and Min Li, "Nonconvex Tensor Relative Total Variation for Image Completion", MDPI (2023).

鏡片棱鏡屈光力自動測量儀的研製

林慶煌 李正忠 吳文弘 詹富貴 簡順源
國立雲林科技大學電子工程學系

摘 要

隨著生活品質的提高，對高品質安全眼鏡和太陽眼鏡的需求不斷增加。棱鏡屈光力是眼鏡測試中重要的項目之一。根據 ISO 18526-1:2020，此測試程序涉及檢查光束穿過眼鏡後將其聚焦在 2 米外的刻度目標上。隨後，透過觀察焦點的位移來確定鏡片的棱鏡屈光力。在測試過程中，可能會涉及人為觀察誤差。本研究開發了機器視覺模組來獲取目標影像，並利用影像處理和識別技術自動確定聚焦光斑的位置並計算每個鏡片的棱鏡屈光力。該儀器消除了人工觀察、手動計算和記錄保存的需要，並減少了檢查所需的勞動力。